

Radar measurements of the axis ratios of cloud particles

Valery Melnikov* and Sergey Matrosov⁺

*-University of Oklahoma, CIMMS, Norman, OK, valery.melnikov@noaa.gov

⁺-CIRES University of Colorado and NOAA Earth Science Research Laboratory, Boulder, CO.

1. Introduction

Cloud particle shapes (habits) affect many cloud properties. Ice particle habits impact crystal growth, evaporation rates, aggregation, fall speeds, and cloud radiative properties. Meteorological radars (e.g., McCormic and Hendry, 1975, Matrosov et al. 2001, 2012, Melnikov and Straka 2013) and lidars (e.g., Neely et al., 2013) with polarization capabilities provide a useful tool for obtaining information on hydrometeor shapes and orientation.

Radars employing the circular polarization scheme provide measurements of the circular depolarization ratio (CDR), which is defined as the logarithmic difference between received signal powers in the co-polarized (P_{co}) and cross-polarized (P_{cr}) channels [i.e., $CDR=10 \log_{10} (P_{co}) - 10 \log_{10} (P_{cr})$].

The analog of CDR in the linear polarization scheme is linear depolarization ratio (LDR). LDR strongly depends on particle shapes and orientations. Compared to LDR, CDR dependence on particle orientation is much weaker (e.g., Matrosov et al. 2001). In fact CDR does not depend on particle orientation in the incident wave polarization plane. This makes CDR a useful parameter for estimating hydrometeor shapes, which are often expressed in terms of particle axis ratios.

Most popular polarimetric radar configuration nowadays is the one with simultaneous transmission and reception (STAR) of horizontally (H) and vertically (V) polarized waves. When hardware phase shifts between H and V channels are known CDR can be approximately estimated from the radar measurements in the STAR mode (e.g., Matrosov 2004). In this study we consider another radar parameter available in the STAR measurement mode, which can be considered as a proxy to CDR and estimations of which do not require accounting for hardware phase shifts and are relatively immune to the propagation effects. A value of this parameter is demonstrated using measurements from the dual-polarization S-band WSR-88D radar operating in the STAR mode.

2. Theoretical basis for estimating the axis ratios of hydrometeors

For the purpose of modeling their scattering properties atmospheric hydrometeors are often modeled as oblate and prolate spheroids (e.g., Bringi and Chandrasekar 2001). The oblate spheroidal model is used for describing planar type hydrometeors (e.g., dendrites, stellars, plates and also raindrops). Columnar particle habits (e.g., columns, bullets, needles) are modeled by prolate spheroids. CDR depends on particle aspect ratios, which for spheroidal model are expressed using minor-to-major axis ratios (b/a). This study suggests a CDR proxy readily available from STAR mode polarimetric measurements and shows the applicability of this proxy for estimating axis ratios.

a. Derivation of the CDR proxy for STAR radar

Fig. 1 presents a sketch of scattering geometry for an oblate particle having the canting angle θ , which is defined as an angle between the vertical axis and the spheroid symmetry axis. The symmetry axis OO' has an angle φ relative to the direction of radar beam designated by the vector \mathbf{k} . \mathbf{E}_h and \mathbf{E}_v are the electric field vectors in the horizontal and vertical planes.

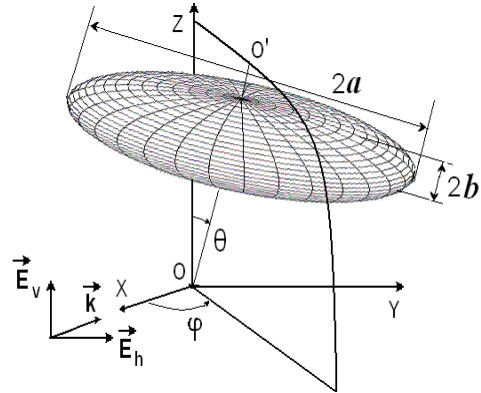


Fig. 1. Geometry of scattering for an oblate particle example.

In the STAR radars, signal paths in the two radar channels with horizontally and vertically polarized waves are different so the transmitted and received waves acquire hardware phase differences on transmission, ψ_t , and reception, ψ_r . A cloud of nonspherical aligned scatterers shifts the phase between the horizontally and vertically polarized waves by the propagation differential phase Φ_{dp} and backscatter differential phase δ so that the measured phase shift is $\psi_{dp} = \psi_t + \psi_r + \Phi_{dp} + \delta$.

For an S-band frequency considered in this study, it is assumed that the backscatter phase δ is negligible and hydrometeors are Rayleigh scatterers. For an ideal antenna, propagation and scattering of polarized waves can be described for the STAR configuration by the following matrix equation (e.g., Melnikov and Straka, 2013) in the backscatter alignment (BSA) convention:

$$\begin{pmatrix} E_{hr} \\ E_{vr} \end{pmatrix} = C \begin{pmatrix} 1 & 0 \\ 0 & \exp[i(\psi_r + \frac{1}{2}\Phi_{dp})] \end{pmatrix} \begin{pmatrix} S_{hh} & S_{hv} \\ S_{hv} & S_{vv} \end{pmatrix} \times \begin{pmatrix} 1 & 0 \\ 0 & \exp[i(\psi_t + \frac{1}{2}\Phi_{dp})] \end{pmatrix} \begin{pmatrix} E_h \\ E_v \end{pmatrix}, \quad (1)$$

where the received wave amplitudes, which are proportional to measured voltages, are on the left side. The amplitude scattering matrix (i.e., S_{ij}) in (1) is bracketed by the matrices, which describe the propagation of the incident wave from the radar to the resolution volume and the propagation of the scattered wave from the radar resolution volume back to the radar. C is a constant which depends on radar parameters and the range to the resolution volume. This constant could be omitted because differential reflectivity Z_{DR} and the copolar correlation coefficient ρ_{hv} , which are used further, do not depend upon it. The radar calibration procedure equalizes the difference in transmitted amplitudes E_h and E_v in (2) so we can assume that they are equal and omit them.

It has been shown (e.g., Holt 1984, Bringi and Chandrasekar 2001, section 3.5.3) that in the absence of propagation differential phase,

$$CDR = 10 \log_{10} \left(\frac{\langle |S_{hh} - S_{vv}|^2 \rangle}{\langle |S_{hh} + S_{vv}|^2 \rangle} \right), \quad (2)$$

where the brackets mean averaging over particle orientation angles and sizes.

The received mean powers $\langle P_h \rangle$, $\langle P_v \rangle$, and signal correlation function $\langle R_{hv} \rangle$ are:

$$\begin{aligned} \langle P_h \rangle &= \langle |E_{hr}|^2 \rangle, & \langle P_v \rangle &= \langle |E_{vr}|^2 \rangle, \\ \langle R_{hv} \rangle &= \langle E_{hr}^* E_{vr} \rangle \end{aligned}, \quad (3)$$

Received voltages in the channels are obtained from (1) as:

$$\begin{aligned} E_{hr} &= S_{hh} + S_{hv} e^{i\psi_t + 0.5i\Phi_{dp}}, \\ E_{vr} &= S_{hv} e^{i\psi_r + 0.5i\Phi_{dp}} + S_{vv} e^{i(\psi_t + \psi_r + \Phi_{dp})}. \end{aligned} \quad (4)$$

Consider the following quantity that is obtained from the latter voltages

$$\frac{\langle |E_{hr} - E_{vr}|^2 \rangle}{\langle |E_{hr} + E_{vr}|^2 \rangle} = \frac{P_h + P_v - 2\text{Re}(R_{hv})}{P_h + P_v + 2\text{Re}(R_{hv})}, \quad (5)$$

Eq. (5) is essentially CDR given by (2) and it also accounts for CDR changes due to differential phase shift on propagation. A following quantity defined here as SDR is free from the phase rotation effects

$$SDR = \frac{P_h + P_v - 2|R_{hv}|}{P_h + P_v + 2|R_{hv}|}. \quad (6)$$

In this SDR notation, ‘‘S’’ that stands for the STAR configuration and ‘‘DR’’ denotes a differential method of its calculation that is seen in (5) and (6). By using (4), the terms in (6) for small δ can be presented as:

$$\begin{aligned} P_h &= \langle |E_{hr}|^2 \rangle = \langle |S_{hh}|^2 \rangle + \\ &2 \cos(\psi_t + 0.5\Phi_{dp}) \text{Re}(\langle S_{hh}^* S_{hv} \rangle) \\ &+ \langle |S_{hv}|^2 \rangle, \end{aligned}$$

$$\begin{aligned} P_v &= \langle |E_{vr}|^2 \rangle = \langle |S_{vv}|^2 \rangle + \\ &2 \cos(\psi_t + 0.5\Phi_{dp}) \text{Re}(\langle S_{vv}^* S_{hv} \rangle) \\ &+ \langle |S_{hv}|^2 \rangle, \end{aligned}$$

$$\begin{aligned} R_{hv} &= \langle E_{hr}^* E_{vr} \rangle = \langle S_{hh}^* S_{hv} \rangle e^{i\psi_r + i0.5\Phi_{dp}} + \\ &\langle S_{hh}^* S_{vv} \rangle e^{i\psi_r + i\psi_t + i\Phi_{dp}} + \\ &\langle |S_{hv}|^2 \rangle e^{i\psi_r - i\psi_t} + \langle S_{hv}^* S_{vv} \rangle e^{i\psi_r + i0.5\Phi_{dp}}. \end{aligned} \quad (7)$$

For the random distribution of φ (i.e., for random orientations of particle axis in the horizontal plane), $\langle S_{hh}^* S_{hv} \rangle = \langle S_{vv}^* S_{hv} \rangle = 0$. Since observed LDR

values in clouds at S-band are usually less than -10 dB, it can be assumed that $|S_{hh}|^2 \gg |S_{hv}|^2$. Then (7) can be rewritten as

$$\begin{aligned} P_h &\approx \langle |S_{hh}|^2 \rangle, & P_v &\approx \langle |S_{vv}|^2 \rangle, \\ R_{hv} &\approx \langle S_{hh}^* S_{vv} \rangle e^{i\psi_t + i\psi_r + i\Phi_{dp}}. \end{aligned} \quad (8)$$

The phase $(\psi_t + \psi_r + \Phi_{dp})$ is the total differential phase measured by a STAR radar. Substitution of (8) into (6) yields

$$SDR = \frac{\langle |S_{hh}|^2 \rangle + \langle |S_{vv}|^2 \rangle - 2 \langle S_{hh}^* S_{vv} \rangle}{\langle |S_{hh}|^2 \rangle + \langle |S_{vv}|^2 \rangle + 2 \langle S_{hh}^* S_{vv} \rangle}. \quad (9)$$

The latter equation can be rewritten in terms of linear Z_{dr} (i.e., $Z_{DR} = 10 \log_{10} Z_{dr}$) and the absolute value of the copolar correlation coefficient ρ_{hv} :

$$SDR = \frac{Z_{dr} + 1 - 2Z_{dr}^{1/2} \rho_{hv}}{Z_{dr} + 1 + 2Z_{dr}^{1/2} \rho_{hv}} \quad (10)$$

In some way, (10) represents a proxy of intrinsic CDR, i.e., a CDR value unaffected by propagation differential phase. SDR is expressed in terms of variables routinely measured by STAR radars. It is seen that (9) is equivalent to (2) expressed in linear units.

b. Modeling results

For Rayleigh scatterers at horizontal incidence, the amplitude scattering matrix elements can be written as [e.g., Bringi and Chandrasekar 2001, eq. (2.53) presented in the BSA convention]

$$\begin{aligned} S_{hh} &= c (\alpha_a + \Delta\alpha \sin^2 \theta \sin^2 \varphi), \\ S_{vv} &= c (\alpha_a + \Delta\alpha \cos^2 \theta), \\ \Delta\alpha &= \alpha_b - \alpha_a, \end{aligned} \quad (11),$$

where α_a and α_b are the polarizabilities of a spheroidal particle along the principal axes and c is a constant, which can be omitted. Substitution of the latter into (8) and then into (9) yields

$$\begin{aligned} SDR &= \frac{\langle |S_{hh} - S_{vv}|^2 \rangle}{\langle |S_{hh} + S_{vv}|^2 \rangle} = \\ &= \frac{\langle |\Delta\alpha|^2 (\sin^2 \theta \sin^2 \varphi - \cos^2 \theta)^2 \rangle}{\langle |2\alpha_a + \Delta\alpha (1 - \sin^2 \theta \cos^2 \varphi)|^2 \rangle}. \end{aligned} \quad (12)$$

For random distribution of particle symmetry axes in the horizontal plane, $\langle \sin^2 \varphi \rangle = 1/2$ and $\langle \sin^4 \varphi \rangle = 3/8$, and (12) reduces to

$$SDR = \frac{\langle |\Delta\alpha|^2 \rangle A}{4 \langle \alpha_a^2 \rangle + 2 \text{Re} \langle \alpha_a \Delta\alpha^2 \rangle + B + \langle |\Delta\alpha|^2 \rangle C}, \quad (13a)$$

$$A = 1 - 3J_1 + J_1^2 + 11J_2/8, \quad (13b)$$

$$B = 2 - J_1, \quad (13c)$$

$$C = 1 - J_1 - J_1^2 + 11J_2/8, \quad (13d)$$

$$J_1 = \langle \sin^2 \theta \rangle, \quad J_2 = \langle \sin^4 \theta \rangle. \quad (13e)$$

Moments J_1 and J_2 can be expressed using the standard deviation of the canting angle σ_θ .

Values of SDR calculated using (13) are presented in Fig. 2a for ice plates and columns. Solid ice with density of 0.92 g cm^{-3} was assumed in the calculations. The Fisher distribution of canting angles was used in calculations of J_1 , J_2 , and σ_θ . Values for $\sigma_\theta = 0^\circ$ correspond to particles oriented with major dimensions in the horizontal plane; $\sigma_\theta = 39^\circ$ is for nearly randomly oriented particles. The mean canting angles for plates is 0° and for columns it is 90° . It is seen from Fig. 2a that SDR depends upon the particle type (plates or columns), the axis ratio, and the magnitude of fluttering σ_θ . Furthermore SDR (as CDR) can be used for estimating axis ratio (b/a) values if particle density is assumed. For instance, if measured SDR is of -20 dB, then b/a lays in an interval from 0.45 to 0.70 for any particle type and fluttering magnitude. If observed SDR values are less than -20 dB, this uncertainty is smaller: for SDR = -25 dB, the interval is $0.65 < b/a < 0.80$, which is a good estimation for the axis ratio. For SDR = -15 dB, the interval is $0.2 < b/a < 0.5$, that also can be used to estimate the axis ratio.

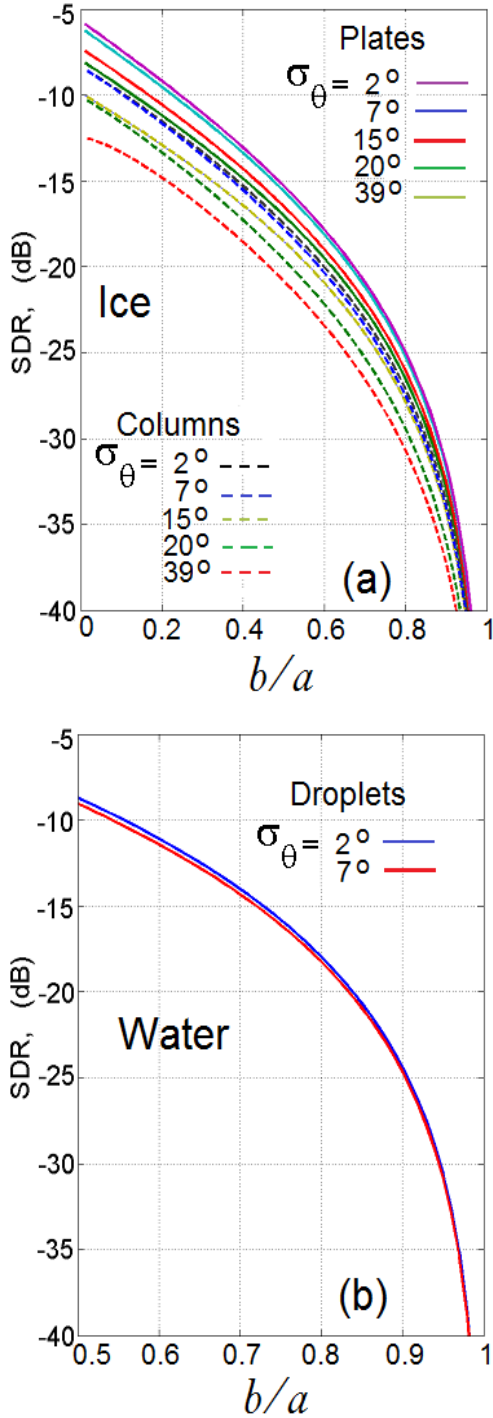


Fig. 2. (a): SDR as a function of b/a for planar (the solid lines) and columar (the dashed lines) ice particles at different intensity of fluttering σ_θ and the elevation angles less than 7° , (i.e., for nearly horizontal incidence). Ice density is 0.92 g cm^{-3} . (b): Same as in (a) but for oblate raindrops.

Modeled SDR values for water drops are shown in Fig. 2b for $\sigma_\theta = 2^\circ$ and 7° . According to measurements by Huang et al. (2008), raindrops experience light fluttering in still air with σ_θ of about 4° .

There is a useful property of SDR that follows from (12): Unlike CDR, SDR is not sensitive to the propagation differential phase. CDR strongly depends on the differential phase Φ_{DP} accumulated during the propagation of radar signals from the radar to the resolution volume and back. As an example, model estimates of CDR as a function of Φ_{DP} are shown in Fig. 3 for the intrinsic CDR value of -21 dB. Changes in the phase on the order of 20° can change CDR by as much as 5 dB. At $\Phi_{DP} > 90^\circ$ and $< 270^\circ$, CDR becomes positive.

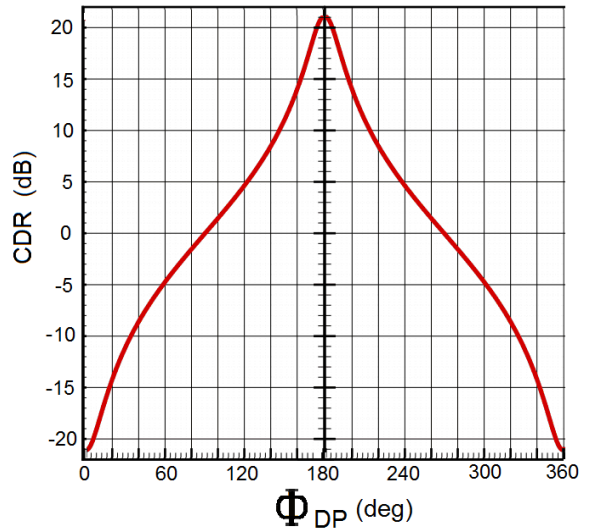


Fig. 3. Estimates of CDR as a function of the propagation differential phase Φ_{DP} for the intrinsic value of -21 dB.

While SDR is immune to Φ_{DP} it can be affected by differential attenuation. In the presence of such attenuation A_{hv} , measured differential reflectivity Z_{DRm} is $Z_{DRm} = A_{hv} Z_{DR}$, where Z_{DR} is the intrinsic differential reflectivity. Differential attenuation can noticeably affect observed differential reflectivity. Since A_{hv} enters into the nominator and denominator of (12), its impact on SDR is less than that for Z_{DR} . Thus the propagation effects should be less pronounced in SDR fields than in Z_{DR} fields. It is demonstrated in the next section using observational data.

3. Observational data

Observational data have been collected with the WSR-88D KOUN radar located at Norman, OK. The dual polarization WSR-88D radars operate in the STAR mode. Figs. 4 and 5 show measurements of reflectivity and differential reflectivity, values of SDR calculated using (10), and SDR-based estimates of hydrometeor axis ratios. One can see in the SDR panels in Fig. 3 and 4 that in regions of ice hydrometeors, SDR changes in a range from about -30 dB (Fig. 4) dB to approximately -7 dB (Fig.5). These experimental results are consistent with model calculations shown in Fig. 2a.

Compare Z_{DR} and SDR fields in Fig. 5. In the Z_{DR} field, one can see radial streaks in the upper part of the echo. This is a usual manifestation of propagation effects with possible impact of oriented crystals near the cloud top. The SDR data in this area exhibit no such patterns, which supports the conclusion made in the previous

section that the propagation effects impact SDR to a lesser extent than Z_{DR} .

Estimations of hydrometeor axis ratios b/a using SDR were performed based on relations presented in Fig. 2 for low antenna elevations. For ice particles located above the melting layer, the median dependence $b/a - SDR$ from the family of curves depicted in Fig. 2a was utilized for these estimations. For higher antenna elevations, similar dependencies have been generated and used for each particular elevation. For raindrops below the melting layer the median dependence of $b/a - SDR$ depicted in Fig. 2b was used. The results are presented in the “Axis Ratio” panels in Figs. 4 and 5. In the melting layer, the axis ratios have been obtained using the relation for water in Fig. 2b assuming that water in the melting particles makes the major contribution to returned signals.

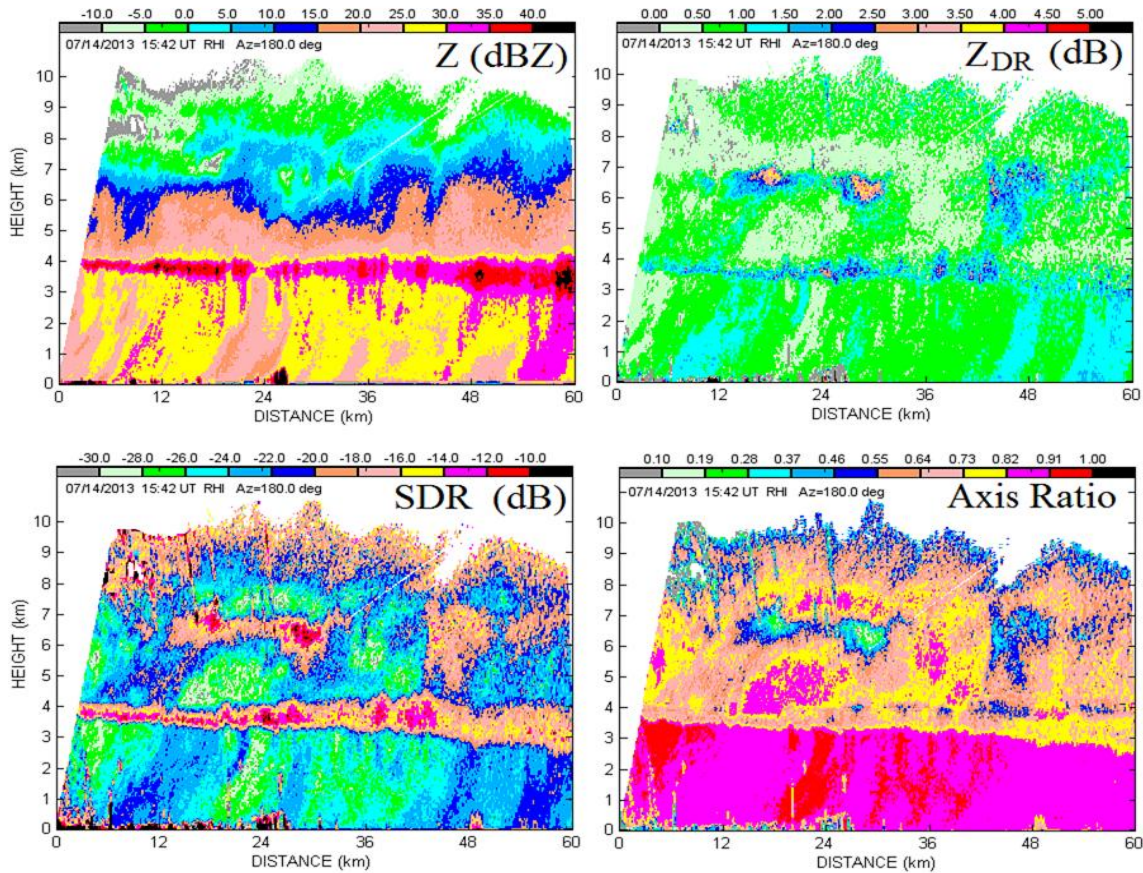


Fig. 4. (left top): Vertical cross-section of reflectivity collected 14 July, 2013 at 1542Z at an azimuth of 180° . (left right, low left, and low right): Corresponding Z_{DR} , SDR, and Axis Ratio fields.

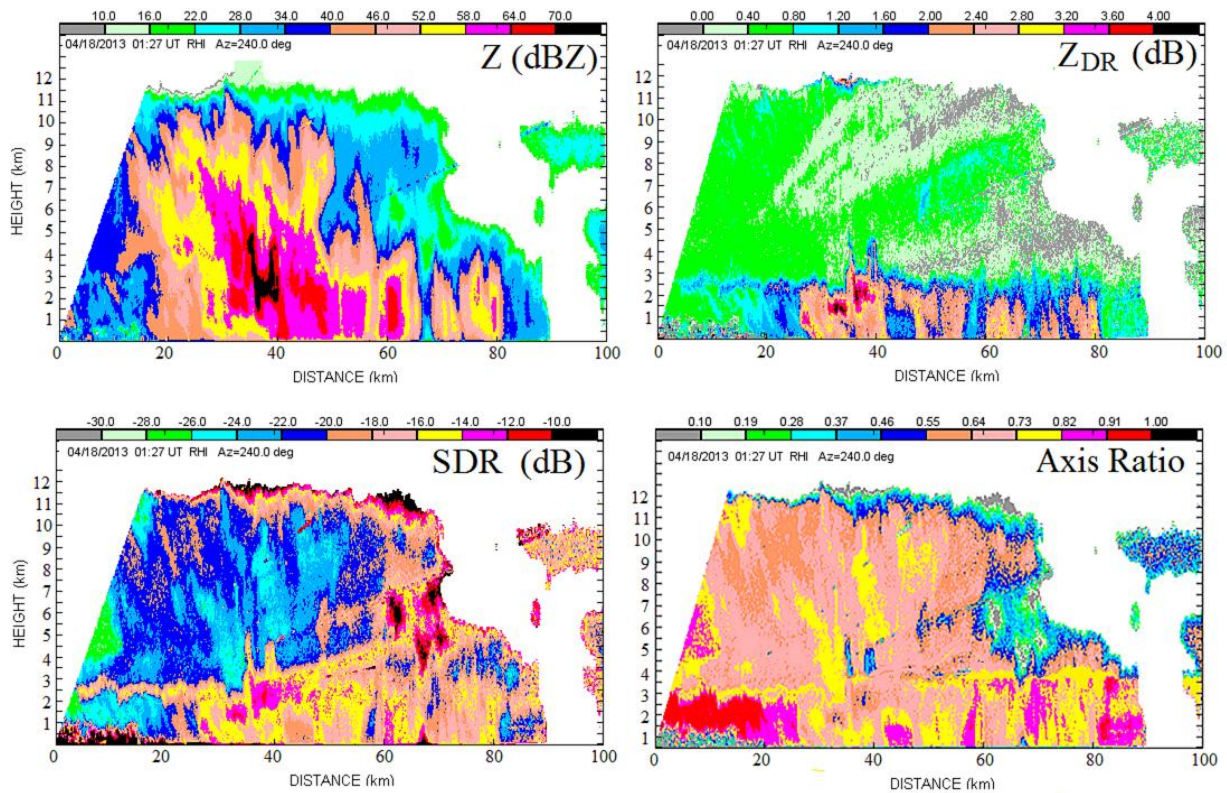


Fig. 5. Same as in Fig. 4 but the data were collected on April 18, 2013 at 0127Z at an azimuth of 240°.

The absence of pronounced SDR radial patterns in the regions, where such patterns are seen in the Z_{DR} field, can be explained, in part, by presence of differential reflectivity values in both nominator and denominator of eq. (10) used for calculating SDR.

An interesting feature is seen in the “Axis Ratio” field in Fig. 5: the axis ratios of 0.3 – 0.4 have been estimated in the area at a distance of 38-40 km and at heights of 4 - 5 km. This area has reflectivities exceeding 70 dBZ, which indicates presence of hail. Z_{DR} in this area is positive. It can be hypothesized that the hailstones there have oblate-like shapes. Such hail shapes have been previously observed in hail-shafts in Oklahoma (e.g., Fig. 6).



Fig. 6. Oblate hailstones collected 10 April 2011 at the KOUN site (a ten cent coin is shown for comparisons).

4. SDR in radar echoes from insects

Modeled SDR values presented in section 2 are based on two assumptions: 1) random distribution of scatterers with their symmetry axes in the horizontal plane (i.e., a random distribution with respect to the azimuthal angle φ , and 2) small $\langle |S_{hv}|^2 \rangle$ in comparison with $\langle |S_{hh}|^2 \rangle$. Further we examine echoes from insects that are strongly aligned scatterers. It is assumed that the returned radar signal is formed primarily by the insects' bodies, which are approximated here with prolate spheroids (Fig. 7). The insects' wings contain little water and their contributions to returned signal can be ignored as the first order of approximation.

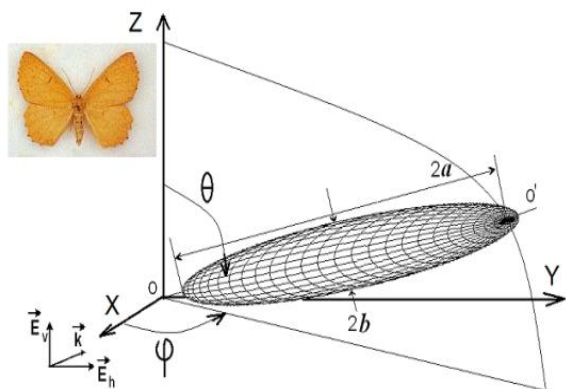


Fig. 7. A picture of a moth (the insert) and geometry of scattering for its body approximated with a prolate spheroid.

Radar echoes from insects usually exhibit strong azimuthal patterns signifying spatial alignment of such scatterers. The azimuthal patterns can be nearly symmetric (e.g., Lang et al. 2004) and strongly asymmetric. The latter case is analyzed herein because it helps to separate effects caused by scatterers (their axis ratios and alignment, and their dielectric permittivity) and effects of radar parameters (the differential phase upon transmission, possible impacts of the backscatter differential phase δ , and the scattering resonances that depend on the size/wavelength ratios).

An example of strongly asymmetric echo is shown in Fig. 8. The reflectivity field in the outer layer (panel Z

in Fig. 8) can be considered as nearly symmetrical relative to a line drawn through the azimuths of 30° and 210° ; the Doppler velocity field exhibits symmetry about this line. Fields of Z_{DR} and Φ_{DP} in the outer layer are more complex and generally asymmetrical.

A scattering model for insects can be based on eq. (1) where preferred alignment and axis ratio of the scatterers are obtained from azimuthal dependencies of Z_{DR} and Φ_{DP} as these parameters do not depend on number concentration of insects in the radar volume. The differential phase on transmit ψ_t is needed to run the model. This phase can be measured in the radar but herein it is a variable of the model. The azimuthal dependencies of Z_{DR} and Φ_{DP} for a circle in the middle of the outer ring in Fig. 8 are depicted in Fig. 9 by the blue lines. The Z_{DR} values from the WSR-88D level II data are represented with one byte (8 bits) in an interval between -7.9 and 7.9 dB. The values outside this interval are truncated by the border values (that is why the blue curve in Fig. 9a has a plateau between about 50° to 150°). Examining the Doppler velocity and Φ_{DP} fields shows that two peaks in Φ_{DP} profile in Fig. 9(b) at azimuths of around 70° and 200° are caused by ground clutter residues.

The variable parameters of the model based on eq. (1) are: the equivalent volume diameter d of the scatterer, the axis ratio b/a of the prolate spheroid, the mean canting angle θ_m of the scatterer, mean orientation angle φ_m , standard deviation of the azimuthal angle distribution, σ_φ , and system differential phase on transmit. Matching the measured Z_{DR} and Φ_{DP} profiles with modeling results allows obtaining parameters indicated above. The model results are shown in Fig. 9 with by the green lines. The observed and modeled Z_{DR} (Fig. 9a) exhibit a good match, whereas the observed differential phase has noticeable deviation from the model curve (Fig. 9b). The match shown in Fig. 9 has been obtained with the following scatterers' parameters: $b/a = 0.4$, $\theta_m = 10^\circ$, $\varphi_m = 20^\circ$, $\sigma_\varphi = 15^\circ$, $\psi_t = 95^\circ$. No variation in θ was introduced. The scattering matrix coefficients were calculated with the T-matrix code described by Mischenko et al. (2002). This model explains the non-symmetric profiles of Z_{DR} and Φ_{DP} . SDR values calculated from STAR measurements using (10) are shown in Fig. 10 with the blue line. The model data with the indicated above parameters are depicted by the green line. Taking into account truncation of large Z_{DR} values at azimuths between about 70° to 150° (Fig. 8a), we can conclude that the model results are in a satisfactory agreement with radar data.

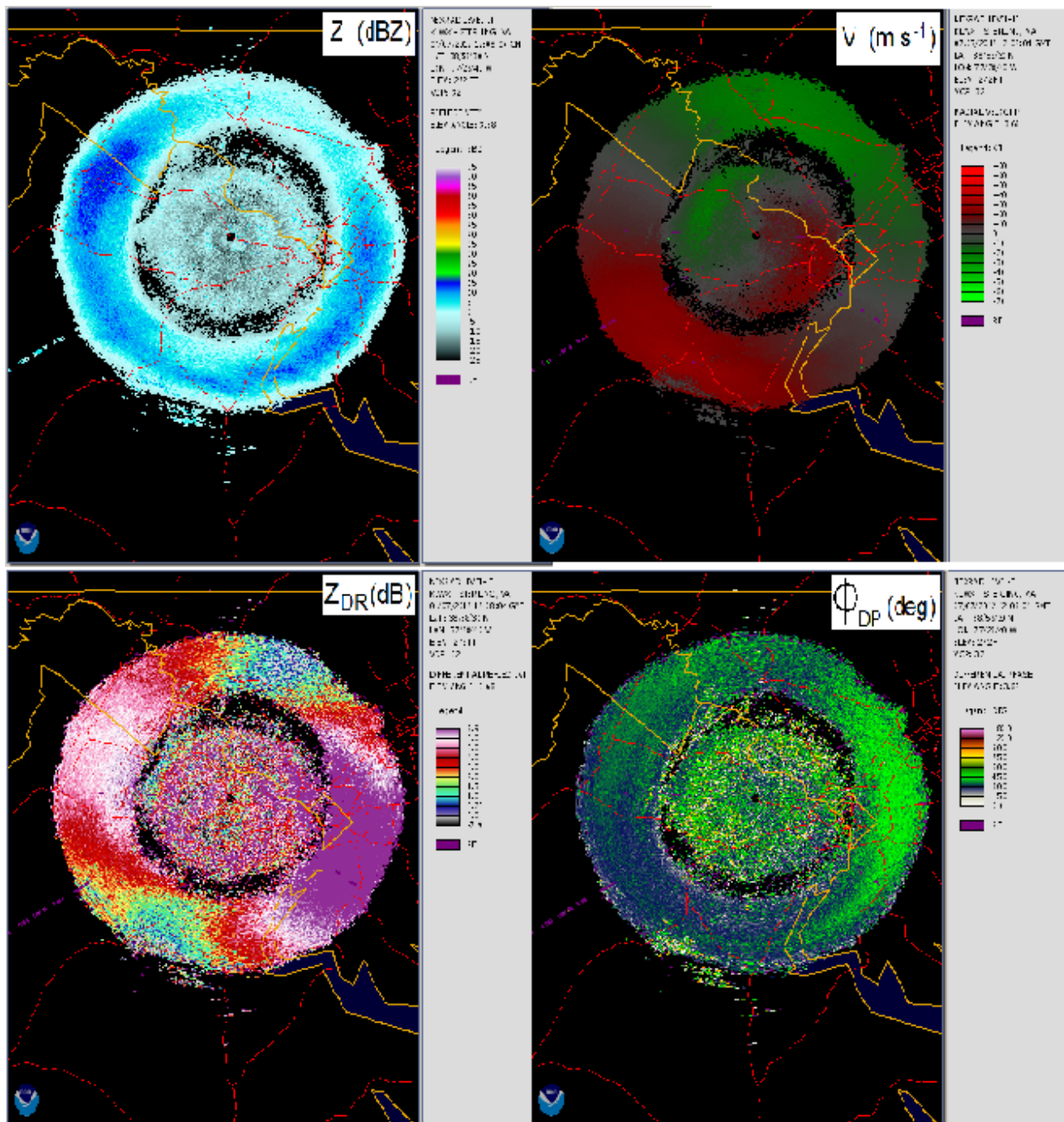


Fig. 8. (left top): Reflectivity field observed with WSR-88D KWLX located in Sterling, VA. The data collected on 07/07/2012 1208Z at an elevation of 3.7° . (top right, bottom left, and bottom right): Same as in the left top panel but for the Doppler velocity, Z_{DR} , and Φ_{DP} .

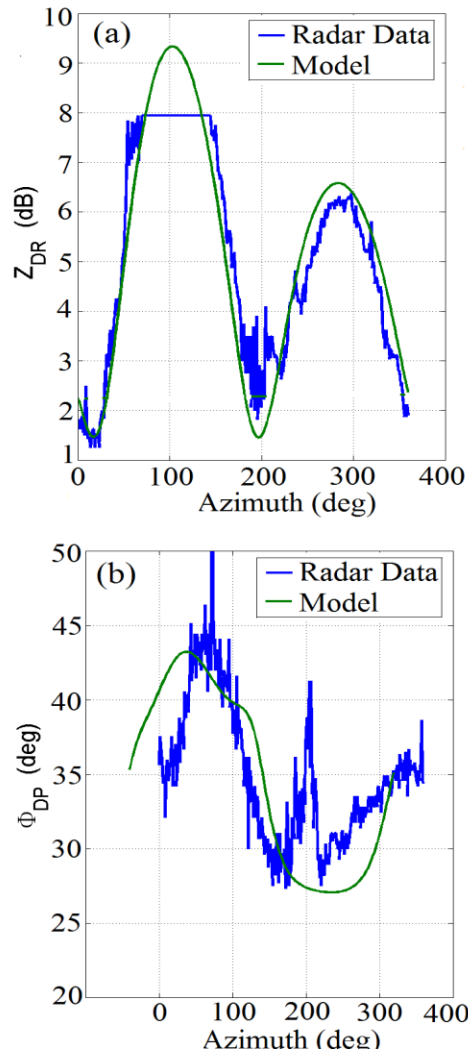


Fig. 9. (a): Azimuthal dependence of Z_{DR} (the blue curve) for the central ring in the outer echo layer in Fig. 6. The green line is the model results. (b): Same as in (a) but for the differential phase.

Most pronounced differences between model and observational data in Figs. 9 and 10 are seen near between azimuths of about 170° to 230° where insects are oriented approximately along the radar beam. In this azimuthal interval, large deviations in Φ_{DP} from the smooth azimuthal dependence are observed (Fig. 9b). These deviations are caused most likely by contamination from ground clutter as was mentioned above. The presented above analysis of insect echo observations provides evidence of a utility of SDR for oriented scatterers.

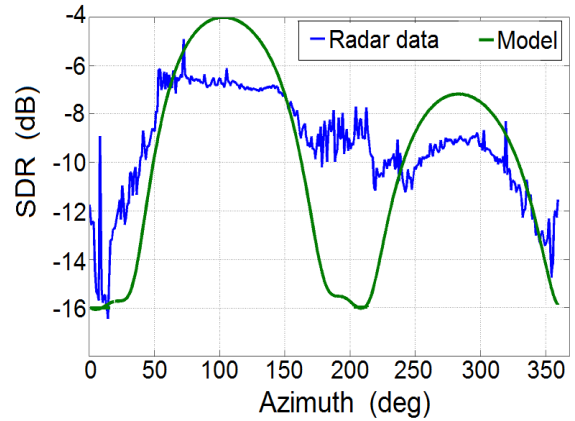


Fig. 10. Values of SDR obtained from radar data (blue line) and modeled data (green curve).

Conclusions

- SDR represents a proxy for intrinsic CDR when the phase propagation influences are effectively removed. SDR depends upon particle shapes (i.e., aspect ratios), orientations, types (e.g., oblate vs prolate) and densities. For particles randomly oriented with their major dimensions approximately in the horizontal plane, the shape dependence is usually the strongest, so information on axis ratios of scatterers can be retrieved if an assumption on their density and phase (i.e., liquid vs ice) are made.
- Values of SDR are calculated using data from polarimetric radars with simultaneous transmission and reception of horizontally and vertically polarized waves. In ice cloud regions, SDR values obtained from polarimetric WSR-88D measurements vary in an interval from about -30 dB to approximately -7 dB which generally corresponds to a wide range of axis ratios (i.e., from very small axis ratio values to almost spherical particles with $b/a \approx 1$).

- CDR is measured with radars employing circular polarization. Copolar echoes for such radars are usually weak which limits the range of CDR observations. SDR is estimated from STAR linear polarization measurements which have two strong returns in receiving channels. This results in longer effective distances for SDR observations.
- SDR exhibits a satisfactory performance in echoes from insects, i.e., for aligned scatterers. Insects are strong scatterers, i.e., they have dielectric permittivity close to the one for water. Reasonable SDR results for strong aligned scatterers make application of SDR more confident for ice particles, which are optically soft scatterers.

References

- Bringi, V. N., and V. Chandrasekar, 2001: *Polarimetric Doppler Weather Radar. Principles and Applications*. Cambridge University Press. 636 pp.
- Holt, A. R., 1984: Some factors affecting the remote sensing of rain by polarization diversity radar in 3- to 35-GHz frequency range. *Radio Sci.*, **47**, 1399–1421.
- Huang G_J., V.N. Bringi, and M. Thurai, 2008: Orientation angle distributions of drops after an 80-m fall using a 2D video disdrometer. *J. Atmos. Oceanic Technol.*, **25**, 1717-1723.
- Lang, T.J., S.A. Rutledge, and J.L. Smith, 2004: Observations of quasi-symmetric echo patterns in clear air with the CSU-CHILL polarimetric radar. *J. Atmos. Oceanic Technol.* **21**, 1182-1189.
- Matrosov, S. Y., 2004: Depolarization estimates from linear H and V measurements with weather radars operating in simultaneous transmission–simultaneous receiving mode. *J. Atmos. Oceanic Technol.*, **21**, 574–583.
- Matrosov, S.Y., R.A. Kropfli, B.E. Marner, and B.W. Bartram, 2001: On the use of radar depolarization ratios for estimating shapes of ice hydrometeors in winter clouds. *J. Appl. Meteor.*, **40**, 479-490.
- Matrosov, S. Y., R. F. Reinking, and I. V. Djalalova, 2005: Inferring fall attitudes of pristine dendritic crystals from polarimetric radar data. *J. Atmos. Sci.*, **62**, 241–250.
- Matrosov, S.Y., G. G. Mace, R. Marchand, M. D. Shupe, A. G. Hallar, I. B. McCubbin, 2012: Observations of Ice Crystal Habits with a Scanning Polarimetric W-Band Radar at Slant Linear Depolarization Ratio Mode. *J. Atmos. Oceanic Technol.*, **29**, 989–1008.
- McCormic, G.C. and Hendry, A. 1975: Principles for the radar determination of the polarization properties of precipitation. *Radio Sci.*, **10**, 421-434.
- Melnikov, V., and J. Straka, 2013: Axis ratios and flutter angles of ice cloud particles: Retrievals from radar data. *J. Atmos. Oceanic Technol.*, **30**, 1691-1703.
- Mischenko, M.I., L.D. Travis, and A.A. Lacis, 2002: *Scattering, Absorption, and Emission of Light by Small Particles*, Cambridge University Press, 228 pp.
- Neely, R.R., M. Hayman, R. Stillwell, J. P. Thayer, R. M. Hardesty, M. O’Neill, M. D. Shupe, C. Alvarez, 2013: Polarization lidar at Summit, Greenland for the detection of cloud phase and particle orientation. *J. Atmos. Oceanic Technol.*, **30**, 1635-1655.